

Adaptive Oscillatory-State Alignment for Time Series Forecasting

Zhangyao Song¹, Ziqiong Li², Xiangfei Qiu³, Chao Zha⁴, Yinfei Xu⁵, Tao Guo¹✉

¹School of Cyber Science and Engineering, Southeast University, Nanjing, China

²School of Mathematics and Statistics, Central South University, Changsha, China

³School of Data Science and Engineering, East China Normal University, Shanghai, China

⁴State Key Laboratory of BlockChain and Data Security, Zhejiang University, Hangzhou, China

⁵School of Information Science and Engineering, Southeast University, Nanjing, China

Abstract—Long-term time series forecasting benefits from inductive biases that expose recurring temporal structure. Existing periodic forecasting methods typically model recurrence through predefined periods, global spectral components, or fixed learnable templates. However, real-world temporal dynamics are rarely rigidly periodic: oscillatory behavior often evolves through amplitude modulation, phase drift, and local frequency variation. Under these conditions, fixed-template periodic modeling can become fundamentally mismatched to the underlying temporal states. We propose AOSNET, a Hilbert-guided forecasting framework that reformulates periodic forecasting from fixed template matching to adaptive oscillatory-state alignment. AOSNET extracts analytic-signal descriptors from both the observed sequence and a learnable global oscillatory prior, then adaptively aligns local states through a descriptor-conditioned gate that selectively preserves reliable observations while softly correcting mismatched regions. The learned prior serves not as a rigid repeated template but as a flexible oscillatory reference interpreted through local state dynamics. Experiments on eight benchmarks demonstrate state-of-the-art or highly competitive accuracy with fast inference speed. Controlled synthetic studies isolating amplitude modulation, phase drift, and local frequency variation confirm that the advantage of oscillatory-state alignment consistently increases as non-stationarity intensifies.

Index Terms—Time series forecasting, periodicity, Hilbert transform, analytic signal, non-stationary time series.

I. INTRODUCTION

Time series forecasting is a fundamental problem in machine learning with broad applications in energy systems, transportation, finance, and climate science [1]–[8]. In long-term forecasting, predictive performance depends not only on modeling short-term dependencies but also on capturing recurring temporal structure over extended horizons [9]–[11]. Consequently, recent research increasingly relies on explicit temporal inductive biases, including decomposition methods, spectral representations, and learnable periodic priors [12]–[14].

Despite their architectural differences, most existing periodic forecasting methods share a common underlying assumption: recurrence can be represented as a fixed repeated template. Some approaches explicitly estimate a dominant period and align observations according to cycle indices [15],

[16]; others model periodicity through global frequency components [12], [17]–[19] or learnable periodic embeddings. Decomposition methods separate seasonal and trend components under similar stationarity assumptions [6], [20]–[22]. These methods have demonstrated strong empirical performance, suggesting that explicit periodic structure is indeed a useful forecasting prior.

The difficulty, however, is not merely that the correct period may be unknown. Many real-world series contain oscillatory behavior whose state changes within a single sequence. Electricity demand may retain a daily rhythm while its intensity varies with weather and human activity; traffic flows may exhibit delayed or advanced peaks under holidays; and environmental signals may contain oscillations whose local pace drifts over time. In these cases, recurring patterns are affected by three coupled factors: amplitude modulation, phase drift, and local frequency variation, which we formally define below.

Definition I.1 (Amplitude Modulation). A signal exhibits *amplitude modulation* if its instantaneous envelope $A(t)$ is not constant over time, i.e., $dA/dt \neq 0$ for some t . In a periodic signal with nominal period P , this means that the peak-to-trough magnitude varies across cycles: the waveform shape repeats but its intensity changes.

Definition I.2 (Phase Drift). A signal exhibits *phase drift* if its instantaneous phase deviates from that of a reference oscillation with constant angular frequency $\omega_0 = 2\pi/P_0$. Formally, defining the phase residual $\delta(t) = \phi(t) - \omega_0 t - \phi_0$, phase drift occurs when $\delta(t)$ is non-constant: $d\delta/dt \neq 0$ for some t . This corresponds to peaks and troughs arriving earlier or later than predicted by the nominal period.

Definition I.3 (Local Frequency Variation). A signal exhibits *local frequency variation* if its instantaneous frequency $\omega(t) = d\phi/dt$ is not constant over time: $d\omega/dt \neq 0$ for some t . Equivalently, the local period $P(t) = 2\pi/\omega(t)$ changes, so consecutive cycles have different durations. This subsumes phase drift as a special case but additionally implies that the rate of phase change itself varies.

These three phenomena are coupled in practice—for instance, a time-varying local period necessarily induces phase drift—but they describe distinct aspects of non-stationarity.

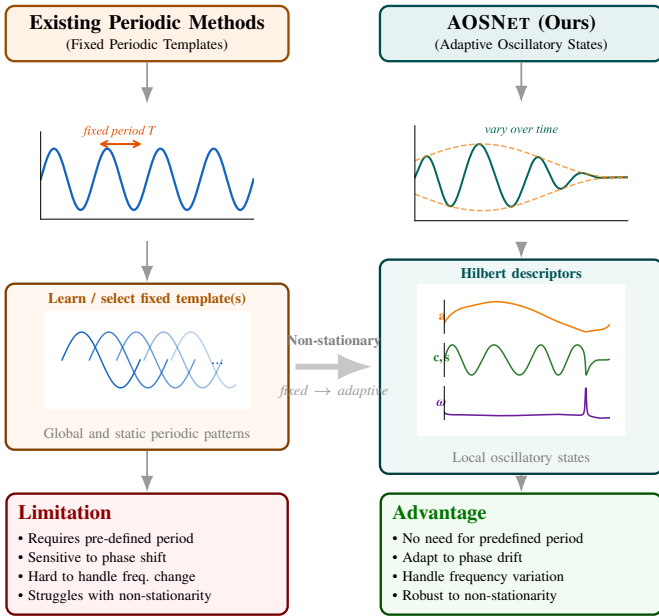


Fig. 1. Motivation of AOSNET. Existing periodic methods typically learn or select fixed periodic templates, which can be sensitive to period misspecification, phase drift, and frequency variation. AOSNET instead represents temporal structure as adaptive local oscillatory states derived from amplitude, phase, and instantaneous-frequency descriptors.

Amplitude modulation changes the signal strength without altering timing; phase drift shifts cycle positions without changing instantaneous speed; and local frequency variation changes the instantaneous oscillation rate. Fixed-template or fixed-period methods assume all three quantities are constant, which motivates the adaptive oscillatory-state alignment of AOSNET.

This observation motivates a different view of periodic forecasting. Rather than treating periodicity as repeated template retrieval, we argue that forecasting should operate in an oscillatory-state space, where recurrence is represented by evolving local dynamical states. The key object is not a globally repeated cycle, but a local oscillatory state describing how strongly the signal oscillates, where it currently lies within the oscillation, and how rapidly the oscillation evolves. These quantities naturally correspond to the amplitude envelope, instantaneous phase, and instantaneous frequency in analytic signal analysis [23], [24]. The Hilbert transform provides differentiable descriptors of these states directly from real-valued sequences, without requiring period selection through prior knowledge, autocorrelation search, or frequency truncation. Fig. 1 illustrates this motivation.

Based on this perspective, we propose AOSNET, a Hilbert-guided forecasting framework for adaptive oscillatory-state alignment. Instead of constructing a cycle table indexed by a predefined period, AOSNET learns a channel-wise global oscillatory prior shared across samples and constructs local oscillatory-state descriptors from both the observed sequence and the prior. A descriptor-conditioned adaptive gate then performs local state alignment by selectively preserving reli-

able observations while softly correcting mismatched regions toward the learned reference. The learned prior does not represent a rigid repeated template; rather, it serves as a flexible oscillatory reference that is adaptively interpreted through local state descriptors.

Concretely, AOSNET derives log-amplitude, phase (sine and cosine), and instantaneous frequency from both the input and the global prior. A lightweight convolutional gate consumes these descriptors and produces a time- and channel-dependent fusion coefficient. After this Hilbert-guided correction, a compact dual-path backbone combines an attention path for cross-variate refinement with a base path for stable temporal projection. The architecture is lightweight, fully differentiable, and requires no manually specified periods.

Our contributions are summarized as follows.

- We reformulate periodic forecasting from fixed template matching to adaptive oscillatory-state alignment, identifying amplitude modulation, phase drift, and local frequency variation as key mismatch sources that fixed-template methods cannot accommodate.
- We propose AOSNET, which compares observations with a learnable global oscillatory prior through Hilbert-domain envelope, phase, and instantaneous-frequency descriptors, then adaptively aligns local states via a descriptor-conditioned gate.
- We demonstrate state-of-the-art or highly competitive accuracy on eight benchmarks with fast inference speed. Controlled synthetic experiments isolating each non-stationary factor confirm that AOSNET consistently outperforms fixed-template baselines, with growing advantage as non-stationarity intensifies.

II. RELATED WORK

1) *Periodic and Decomposition-Based Forecasting*: Long-term forecasting has increasingly relied on explicit temporal-structure modeling. Attention- and convolution-based architectures enlarge the receptive field for long-range dependencies [5], [9], [10], [25], [26], while lightweight decomposition methods prove highly competitive [6], [20], [21], [27]. More recently, learnable periodic priors have emerged as strong forecasting inductive biases: CycleNet learns recurrent cycle templates [15], TQNet injects periodically shifted learnable vectors as temporal queries [16], and MoFo models periodic patterns for long-term prediction [28]. These methods share a common assumption—recurrence is represented as a fixed repeated template indexed by a predefined or estimated period. When the underlying oscillatory dynamics evolve through amplitude modulation, phase drift, or frequency variation, this fixed-template assumption becomes a fundamental limitation. AOSNET departs from this paradigm by performing adaptive oscillatory-state alignment through Hilbert-domain descriptors, preserving the benefit of explicit temporal priors without requiring globally stable periods.

2) *Frequency-Domain and Signal-Processing Methods*: Frequency-domain approaches exploit the spectral separability of periodic structure. FEDformer and FILM model

long-range dependencies via frequency representations [17], [25]; FITS performs lightweight frequency interpolation [29]; FAN addresses non-stationarity through frequency-adaptive normalization [12]; FreDF learns directly in the frequency domain [18]; and Amplifier recovers neglected low-energy components [19]. While effective, these methods operate on global or window-level spectral components and thus implicitly assume locally stationary frequency content. AOSNET instead derives time-local analytic-signal descriptors—envelope, instantaneous phase, and instantaneous frequency—via the Hilbert transform [23], [24]. This enables modeling of amplitude modulation and frequency drift at each time step, providing finer-grained oscillatory-state information than global spectral decomposition.

3) *Multivariate Dependency Modeling*: Cross-variate dependency modeling complements temporal modeling in multivariate forecasting. Early Transformer variants mix temporal and channel dimensions through attention [5], [9], [30], [31]; PatchTST advocates channel independence for robustness [10]; and subsequent work revisits the independence-versus-interaction trade-off [32]. Inverted or channel-token architectures—iTransformer [11], Crossformer [33], HD-Mixer [34], SAMformer [35]—further advance multivariate interaction learning. These methods focus on how variables interact after representation, yet the temporal signal fed into cross-variate modules may still carry non-stationary oscillatory distortions. AOSNET addresses this by first performing per-channel oscillatory-state alignment, so that downstream channel-token attention operates on structurally refined signals rather than raw observations.

III. METHODOLOGY

This section presents AOSNET, a Hilbert-guided forecasting framework that reformulates periodic modeling from fixed template matching to adaptive oscillatory-state alignment. We first define the forecasting problem, then introduce the analytic-signal descriptors, and finally describe the adaptive oscillatory-state (AOS) module and forecasting backbone.

A. Problem Formulation

Given a multivariate historical window $\mathbf{X} \in \mathbb{R}^{C \times L}$ with C variables and look-back length L , the goal of point forecasting is to predict the future horizon $\mathbf{Y} \in \mathbb{R}^{C \times H}$:

$$f_{\theta} : \mathbf{X}_{t-L+1:t} \mapsto \widehat{\mathbf{Y}}_{t+1:t+H}, \quad (1)$$

where H is the forecasting length. For notation clarity, we omit the time index and write the input as \mathbf{X} and the prediction as $\widehat{\mathbf{Y}}$. AOSNET follows the channel-token convention commonly used in multivariate forecasting: each variate is first represented as an individual temporal token, and cross-variate dependencies are refined after oscillatory-state alignment.

B. Analytic-Signal Descriptors

The core idea of AOSNET is to represent temporal dynamics in an oscillatory-state space rather than through a fixed

global period. For a real-valued sequence $\mathbf{x} \in \mathbb{R}^L$, its analytic signal is defined as

$$\mathbf{z} = \mathbf{x} + i \mathcal{H}(\mathbf{x}), \quad (2)$$

where $\mathcal{H}(\cdot)$ denotes the Hilbert transform [23], [24]. In practice, we compute it with an FFT-based differentiable implementation [36]. Let \mathcal{F} and \mathcal{F}^{-1} denote the discrete Fourier transform and its inverse. The analytic signal can be obtained by suppressing negative frequencies and doubling positive frequencies:

$$\mathbf{z} = \mathcal{F}^{-1}(\mathbf{m} \odot \mathcal{F}(\mathbf{x})), \quad (3)$$

where $\mathbf{m} \in \mathbb{R}^L$ is the standard analytic-signal frequency mask. For even L , $m_0 = m_{L/2} = 1$, $m_k = 2$ for $1 \leq k < L/2$, and the remaining entries are zero; the odd-length case is defined analogously.

From \mathbf{z} , we extract three local descriptors:

$$\mathbf{a} = \log(|\mathbf{z}| + \epsilon), \quad (4)$$

$$\mathbf{c} = \cos(\angle \mathbf{z}), \quad \mathbf{s} = \sin(\angle \mathbf{z}), \quad (5)$$

$$\omega_{\ell} = \angle(z_{\ell} z_{\ell-1}^*), \quad \ell = 2, \dots, L. \quad (6)$$

Here \mathbf{a} is the log-amplitude envelope, (\mathbf{c}, \mathbf{s}) provides a continuous phase representation, and ω estimates instantaneous frequency through phase increments. The first frequency value is padded by replication. The phase-increment form avoids explicit phase unwrapping and yields a bounded local descriptor of instantaneous frequency. These descriptors are used as structural cues; they do not require the signal to have a single stable cycle.

C. Adaptive Oscillatory-State Alignment

AOSNET performs adaptive oscillatory-state alignment through descriptor-conditioned interpolation between the observed sequence and a learnable oscillatory reference.

1) *Global Oscillatory Prior*: AOSNET introduces a learnable channel-wise prior $\mathbf{P} \in \mathbb{R}^{C \times L}$, shared across all samples. Unlike fixed periodic templates indexed by a predefined period, \mathbf{P} is not constrained to repeat with any cycle length. It serves as a flexible oscillatory reference that is adaptively interpreted through local state descriptors, with its influence modulated by the gate at each time step.

2) *Descriptor-conditioned gate*: For each input \mathbf{X} , we compute analytic-signal descriptors for both the observed sequence and the global temporal prior:

$$\mathcal{D}(\mathbf{X}) = \{\mathbf{a}^x, \mathbf{c}^x, \mathbf{s}^x, \omega^x\}, \quad \mathcal{D}(\mathbf{P}) = \{\mathbf{a}^p, \mathbf{c}^p, \mathbf{s}^p, \omega^p\}. \quad (7)$$

For each channel, we concatenate these descriptors along the feature dimension:

$$\mathbf{u}_c = \text{Concat}[\mathbf{a}_c^x, \mathbf{a}_c^p, \mathbf{c}_c^x, \mathbf{s}_c^x, \mathbf{c}_c^p, \mathbf{s}_c^p, \omega_c^x, \omega_c^p] \in \mathbb{R}^{8 \times L}. \quad (8)$$

A lightweight one-dimensional convolutional gate then produces a local fusion coefficient:

$$\mathbf{g}_c = \sigma(\text{Conv}_2(\phi(\text{Conv}_1(\mathbf{u}_c))))), \quad \mathbf{g}_c \in [0, 1]^L, \quad (9)$$

where $\phi(\cdot)$ is the GELU (Gaussian Error Linear Unit) activation [37] and $\sigma(\cdot)$ is the sigmoid function.

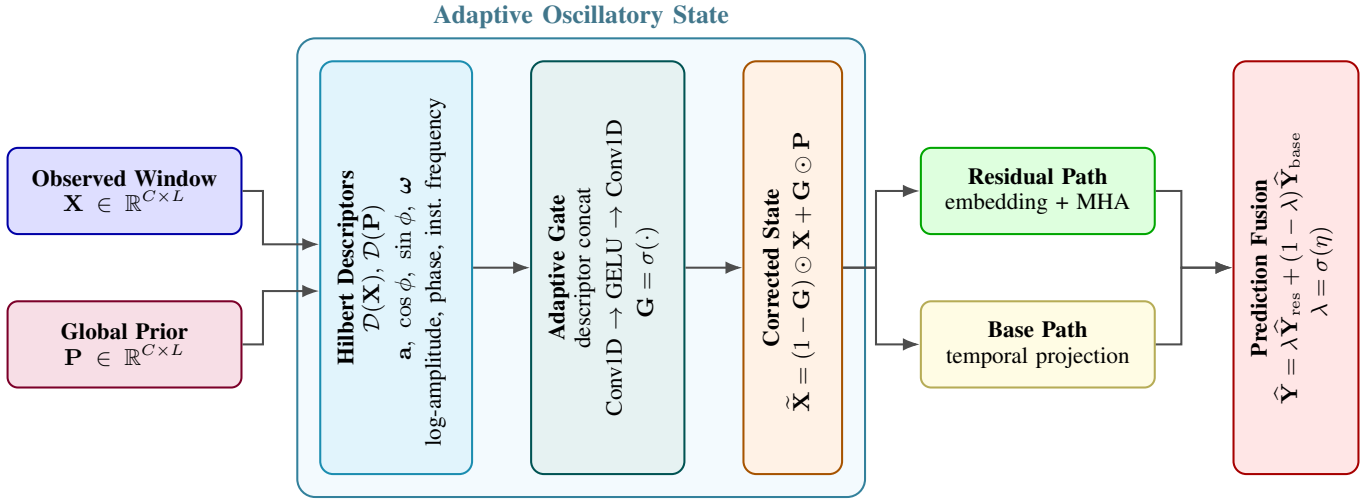


Fig. 2. Overall architecture of AOSNET. The observed sequence and a learnable global oscillatory prior are mapped to analytic-signal descriptors, from which a descriptor-conditioned gate performs adaptive oscillatory-state alignment. The aligned representation is processed by two complementary forecasting paths: an attention path with channel-token attention, and a base path with direct temporal projection, fused by a learnable coefficient.

3) *State Alignment*: The gate performs local oscillatory-state alignment by adaptively interpolating between the observation and the global oscillatory prior:

$$\tilde{\mathbf{X}} = (1 - \mathbf{G}) \odot \mathbf{X} + \mathbf{G} \odot \mathbf{P}, \quad (10)$$

where $\mathbf{G} \in [0, 1]^{C \times L}$ stacks all channel gates. When the observed oscillatory state is locally consistent with the learned prior, the gate preserves the raw sequence; when amplitude, phase, or frequency descriptors indicate a mismatch, the model softly corrects the input toward \mathbf{P} . This mechanism provides an explicit temporal inductive bias through gated residual alignment rather than fixed period indexing or hard template matching.

D. Dual-Path Forecasting Head

After oscillatory-state alignment, AOSNET feeds the aligned sequence $\tilde{\mathbf{X}} \in \mathbb{R}^{C \times L}$ into two complementary forecasting paths (see Fig. 2). The two paths separate stable per-channel temporal extrapolation from expressive cross-variate refinement, so that the primary temporal inductive bias remains in the AOS module rather than being absorbed into a more complex backbone.

1) *Attention Path*: This path models cross-variate nonlinear corrections after alignment. A shared temporal embedding first projects each channel from the look-back length L into a hidden dimension d , with dropout regularization [38]:

$$\mathbf{h}_c = \text{Dropout}(\phi(\mathbf{W}_e \tilde{\mathbf{x}}_c + \mathbf{b}_e)), \quad \mathbf{h}_c \in \mathbb{R}^d. \quad (11)$$

Stacking all channels gives $\mathbf{H} \in \mathbb{R}^{C \times d}$. A residual multi-head self-attention (MHA) layer [30] then refines cross-variate interactions over these channel tokens:

$$\mathbf{R} = \text{MHA}(\mathbf{H}, \mathbf{H}, \mathbf{H}) + \mathbf{H}. \quad (12)$$

The refined features are passed through a shallow nonlinear projection and output head:

$$\hat{\mathbf{Y}}_{\text{att}} = \mathbf{W}_o \phi(\mathbf{W}_r \mathbf{R} + \mathbf{b}_r) + \mathbf{b}_o. \quad (13)$$

2) *Base Path*: This path provides the stable per-channel extrapolation anchor. For each channel, a shared weight matrix directly maps the corrected look-back window to the prediction horizon:

$$\hat{\mathbf{y}}_{\text{base},c} = \mathbf{W}_l \tilde{\mathbf{x}}_c + \mathbf{b}_l, \quad \mathbf{W}_l \in \mathbb{R}^{H \times L}. \quad (14)$$

Stacking all channels gives $\hat{\mathbf{Y}}_{\text{base}} \in \mathbb{R}^{C \times H}$.

3) *Prediction Fusion*: The final prediction is a learnable combination of the two paths:

$$\hat{\mathbf{Y}} = \lambda \hat{\mathbf{Y}}_{\text{att}} + (1 - \lambda) \hat{\mathbf{Y}}_{\text{base}}, \quad \lambda = \sigma(\eta), \quad (15)$$

where η is a scalar learnable parameter. This dual-path design lets the model adaptively allocate prediction mass between stable channel-wise extrapolation in the base path and nonlinear cross-variate correction in the attention path.

IV. FFT-BASED ANALYTIC SIGNAL IMPLEMENTATION

Algorithm 1 summarizes the analytic-signal computation for a single real-valued sequence. The frequency mask preserves the DC component, preserves the Nyquist component for even-length sequences, doubles positive frequencies, and removes negative frequencies.

We provide a self-contained derivation of the Hilbert transform and its connection to the analytic-signal descriptors used in AOSNET.

1) *Continuous-Time Definition*: For a real-valued signal $x(t) \in L^2(\mathbb{R})$, the Hilbert transform is defined as the Cauchy principal value integral [23]:

$$\mathcal{H}\{x\}(t) = \frac{1}{\pi} \text{p.v.} \int_{-\infty}^{\infty} \frac{x(\tau)}{t - \tau} d\tau = \left(\frac{1}{\pi t} \right) * x(t), \quad (16)$$

where $*$ denotes convolution. Intuitively, the Hilbert transform is an all-pass filter that shifts each frequency component of $x(t)$ by $-\pi/2$ radians while preserving its amplitude.

Algorithm 1 FFT-Based Analytic Signal for One Sequence

1: **Input:** Real-valued sequence $\mathbf{x} = (x_0, \dots, x_{L-1}) \in \mathbb{R}^L$
2: **Output:** Analytic signal $\mathbf{z} \in \mathbb{C}^L$
3: $\mathbf{s} \leftarrow \mathcal{F}(\mathbf{x})$ (Fourier spectrum)
4: $\mathbf{m} \leftarrow \mathbf{0} \in \mathbb{R}^L$ (Frequency mask)
5: **if** L is even **then**
6: $m_0 \leftarrow 1, m_{L/2} \leftarrow 1$
7: $m_k \leftarrow 2$ for $k = 1, \dots, L/2 - 1$
8: **else**
9: $m_0 \leftarrow 1$
10: $m_k \leftarrow 2$ for $k = 1, \dots, (L-1)/2$
11: **end if**
12: $\mathbf{z} \leftarrow \mathcal{F}^{-1}(\mathbf{m} \odot \mathbf{s})$
13: **return** \mathbf{z}

2) *Frequency-Domain Interpretation:* Let $X(f) = \mathcal{F}\{x\}(f)$ denote the Fourier transform of $x(t)$. The transfer function of the Hilbert transform is

$$H(f) = \mathcal{F}\left\{\frac{1}{\pi t}\right\} = -i \operatorname{sgn}(f) = \begin{cases} -i, & f > 0, \\ 0, & f = 0, \\ +i, & f < 0, \end{cases} \quad (17)$$

so the Fourier transform of the Hilbert-transformed signal is

$$\mathcal{F}\{\mathcal{H}\{x\}\}(f) = -i \operatorname{sgn}(f) \cdot X(f). \quad (18)$$

This confirms the $-\pi/2$ phase shift: multiplying by $-i$ rotates the phasor by -90° for positive frequencies and by $+90^\circ$ for negative frequencies.

3) *Construction of the Analytic Signal:* The analytic signal is formed by combining the original signal with its Hilbert transform as the imaginary part:

$$z(t) = x(t) + i \mathcal{H}\{x\}(t). \quad (19)$$

Taking the Fourier transform of both sides:

$$\begin{aligned} Z(f) &= X(f) + i \cdot [-i \operatorname{sgn}(f)] X(f) \\ &= X(f) [1 + \operatorname{sgn}(f)] \\ &= \begin{cases} 2X(f), & f > 0, \\ X(0), & f = 0, \\ 0, & f < 0. \end{cases} \end{aligned} \quad (20)$$

Thus, the analytic signal retains only positive-frequency content (doubled in magnitude) and removes negative frequencies entirely. This one-sided spectrum ensures that the instantaneous amplitude, phase, and frequency are uniquely and meaningfully defined.

4) *Instantaneous Amplitude (Envelope):* The instantaneous amplitude is the modulus of the analytic signal:

$$A(t) = |z(t)| = \sqrt{x(t)^2 + \mathcal{H}\{x\}(t)^2}. \quad (21)$$

This quantity traces the envelope of the oscillation. In AOSNET, we use the log-amplitude $\mathbf{a} = \log(|\mathbf{z}| + \epsilon)$ for numerical stability and to normalize scale differences across channels.

5) *Instantaneous Phase:* The instantaneous phase is the argument of the analytic signal:

$$\phi(t) = \angle z(t) = \arctan \frac{\mathcal{H}\{x\}(t)}{x(t)}. \quad (22)$$

Rather than using $\phi(t)$ directly (which requires unwrapping to avoid 2π discontinuities), AOSNET represents phase through its sine and cosine components ($\cos \phi, \sin \phi$). This provides a continuous, bounded representation on the unit circle that is compatible with gradient-based optimization.

6) *Instantaneous Frequency:* The instantaneous frequency is the time derivative of the instantaneous phase:

$$\omega(t) = \frac{d\phi(t)}{dt}. \quad (23)$$

For discrete sequences, we approximate this via the phase increment between consecutive samples. Using the property that for two complex numbers z_ℓ and $z_{\ell-1}$, the phase difference equals the argument of their product with conjugate:

$$\omega_\ell = \phi_\ell - \phi_{\ell-1} = \angle(z_\ell \cdot z_{\ell-1}^*), \quad \ell = 2, \dots, L, \quad (24)$$

where z^* denotes complex conjugation. This formulation avoids explicit phase unwrapping because $\angle(z_\ell z_{\ell-1}^*)$ is always in $(-\pi, \pi]$, yielding a bounded descriptor that directly measures local oscillation speed.

7) *Summary:* The three descriptors—log-amplitude \mathbf{a} , phase $(\mathbf{c}, \mathbf{s}) = (\cos \angle \mathbf{z}, \sin \angle \mathbf{z})$, and instantaneous frequency ω —together characterize the local oscillatory state of a signal at each time step. They are computed entirely through FFT operations (Algorithm 1) and are fully differentiable, making them suitable as conditioning inputs to the adaptive gate in AOSNET.

V. EXPERIMENTS

We conduct a comprehensive empirical evaluation of AOSNET across five complementary axes. First, we benchmark forecasting accuracy against nine recent models on eight standard datasets (Sec. V-B). Second, we construct a controlled setting where fixed-template methods systematically fail under amplitude-phase perturbations, illustrating the motivation behind adaptive oscillatory-state alignment (Sec. V-C). Third, we analyze the learned representations to verify that the global prior functions as an oscillatory reference rather than a rigid template, and that the gate operates meaningfully in the envelope-phase-frequency space (Sec. V-D). Fourth, a case study demonstrates that two time windows with identical phase can nonetheless require distinct oscillatory states (Sec. V-E). Fifth, we evaluate on two workload traces from a cloud-service benchmark to test whether the same alignment story transfers to operational load forecasting (Sec. V-B2). Finally, we ablate each component and examine sensitivity to key hyperparameters (Sec. V-F).

TABLE I

DETAILED INFORMATION ABOUT THE DATASETS USED IN THIS STUDY.

Dataset	Channels	Timesteps	Interval	Domain
<i>Common Benchmarks</i>				
ETTh1	7	14,400	1 hour	Electricity
ETTh2	7	14,400	1 hour	Electricity
ETTh1	7	57,600	15 mins	Electricity
ETTh2	7	57,600	15 mins	Electricity
Electricity	321	26,304	1 hour	Electricity
Solar	137	52,560	10 mins	Energy
Traffic	862	17,544	1 hour	Transportation
Weather	21	52,696	10 mins	Weather
<i>Workload Traces</i>				
IaaS	93	3,456	10 mins	Cloud workload
PaaS	426	7,776	10 mins	Cloud workload

A. Setup

All experiments are implemented in PyTorch [39]. We evaluate forecasting accuracy with Mean Squared Error (MSE) and Mean Absolute Error (MAE), where lower values indicate better performance. Following the standard long-term forecasting protocol, the look-back length is fixed to $L = 96$ for all benchmark comparisons.

1) *Datasets*: We evaluate on 8 widely-used multivariate forecasting benchmarks: ETTh1, ETTh2, ETTm1, ETTm2 from the ETT series [5]; Electricity, Solar-Energy, Traffic, and Weather [9]. We further evaluate on two cloud workload traces (IaaS and PaaS) sampled at 10-minute intervals. For all datasets, the prediction horizons are $H \in \{96, 192, 336, 720\}$ with a fixed look-back length of 96. Detailed dataset statistics are summarized in Table I.

2) *Baselines*: We compare AOSNET with representative recent forecasting models, including TQNet [16], SRSNet [40], SSformer [41], CycleNet [15], Amplifier [19], iTransformer [11], PatchTST [10], and DLinear [6]. To ensure consistency with the reference benchmark, we use TQNet’s reported results when available and supplement missing baseline entries from SEER; SSformer results are taken from the original paper. When the two sources overlap, TQNet is treated as the primary source.

B. Forecasting Performance

1) *Common Benchmarks*: Table II reports the full results across all horizons. AOSNET achieves the best or second-best MSE on 7 out of 8 datasets and the best MAE on 7 out of 8 datasets; the only exceptions are Solar-Energy (where the best MSE belongs to TQNet) and Traffic (where the best MAE belongs to TQNet). Compared with the most relevant fixed-template periodic-prior baselines (TQNet, CycleNet), AOSNET consistently improves accuracy, particularly on datasets with complex oscillatory dynamics such as Electricity (-3.0% MSE vs. TQNet) and ETTh2 (-4.8% MSE vs. TQNet). These gains are consistent with our motivation: adaptive oscillatory-state alignment is most beneficial when recurrence persists but local amplitude, phase, or frequency states evolve over time.

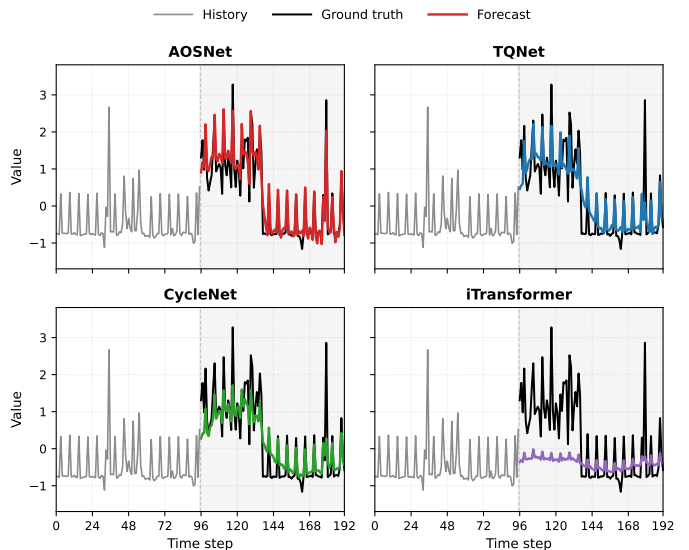


Fig. 3. Representative IaaS 96→96 forecasting visualization on a single channel. Each panel compares the same history window (gray), ground truth (black), and model forecast (colored) for AOSNET, TQNet, CycleNet, and iTransformer. AOSNET tracks the post-history state transition more faithfully, whereas the baselines either over-smooth the change point or drift toward rigid template-like forecasts.

2) *Workload Forecasting*: We further evaluate on two cloud workload traces (IaaS and PaaS) sampled every 10 minutes. In addition to MSE and MAE, we report Normalized MAE (NMAE). Table III presents the full per-horizon results. AOSNET ranks first on all metrics for IaaS and on average for PaaS, with the advantage over TQNet growing at longer horizons (MSE gap from 0.000 at $H=96$ to 0.043 at $H=720$ on IaaS). This confirms that adaptive oscillatory-state alignment transfers effectively to operational cloud workload forecasting.

Fig. 3 shows a representative IaaS 96→96 case. On this sample, AOSNET follows the post-history regime transition more faithfully, while TQNet and CycleNet remain closer to rigid template-like dynamics and iTransformer underfits the oscillatory pattern.

3) *Stability*: To assess statistical significance, we report all AOSNET results as the mean and standard deviation over 5 independent runs with different random seeds. As shown in Table II, the standard deviations are tightly bounded across all datasets and horizons—MSE std is at most 0.003 and MAE std at most 0.003—indicating that AOSNET’s performance is stable and not sensitive to random initialization.

4) *Efficiency*: Fig. 4 shows that AOSNET achieves the best accuracy–efficiency trade-off: lowest MSE/MAE with the fastest inference (9.15 ms/batch)— $1.4\times$ faster than TQNet, $7.9\times$ faster than PatchTST, and $17.6\times$ faster than SSformer—while using only 1.45M parameters.

C. Failure Modes of Fixed-Template Periodicity

The introduction argues that fixed periodic templates become fundamentally mismatched under amplitude modulation, phase drift, and local frequency variation. We now provide

TABLE II

FULL MULTIVARIATE FORECASTING RESULTS FOR ALL PREDICTION HORIZONS. THE LOOK-BACK LENGTH IS FIXED TO 96. AOSNET VALUES ARE MEAN \pm STD OVER 5 RUNS.

Model	AOSNET (Ours)		TQNet (2025)		SRSNet (2025)		SSformer (2026)		CycleNet (2024)		Amplifier (2025)		iTransformer (2024)		PatchTST (2023)		DLinear (2023)		
	MSE	MAE	MSE	MAE	MSE	MAE	MSE	MAE	MSE	MAE	MSE	MAE	MSE	MAE	MSE	MAE	MSE	MAE	
ETTh1	96	0.368 \pm 0.002	0.392 \pm 0.001	<u>0.371</u>	<u>0.393</u>	0.383	0.395	0.373	0.393	0.375	0.395	0.376	0.393	0.386	0.405	0.414	0.419	0.386	0.400
	192	0.421 \pm 0.003	0.421 \pm 0.002	<u>0.428</u>	<u>0.426</u>	0.433	0.422	0.432	0.431	0.436	0.428	0.442	0.430	0.441	0.436	0.460	0.445	0.437	0.432
	336	0.459 \pm 0.002	0.440 \pm 0.003	0.476	0.446	0.476	0.446	0.483	0.454	0.496	0.455	0.478	0.446	0.487	0.458	0.501	0.466	0.481	0.459
	720	0.462 \pm 0.003	0.461 \pm 0.002	0.487	<u>0.470</u>	<u>0.474</u>	0.471	0.519	0.495	0.520	0.484	0.501	0.479	0.503	0.491	0.500	0.488	0.519	0.516
	Avg	0.427 \pm 0.003	0.429 \pm 0.002	<u>0.441</u>	0.434	0.442	<u>0.433</u>	0.452	0.443	0.457	0.441	0.449	0.437	0.454	0.448	0.469	0.455	0.456	0.452
ETTh2	96	0.280 \pm 0.002	0.329 \pm 0.002	0.295	0.343	0.296	0.345	<u>0.281</u>	<u>0.332</u>	0.298	0.344	0.298	0.347	0.297	0.349	0.302	0.348	0.333	0.387
	192	0.354 \pm 0.003	0.378 \pm 0.001	<u>0.367</u>	0.393	0.369	0.392	<u>0.367</u>	<u>0.385</u>	0.372	0.396	0.378	0.401	0.380	0.400	0.388	0.400	0.477	0.476
	336	0.396 \pm 0.001	0.414 \pm 0.002	0.417	0.427	0.413	0.425	0.394	0.418	0.431	0.439	0.428	0.437	0.428	0.432	0.426	0.433	0.594	0.541
	720	<u>0.410</u> \pm 0.002	<u>0.428</u> \pm 0.003	0.433	0.446	0.425	0.444	0.395	0.420	0.450	0.458	0.452	0.460	0.427	0.445	0.431	0.446	0.831	0.657
	Avg	<u>0.360</u> \pm 0.002	0.387 \pm 0.002	0.378	0.402	0.376	0.402	0.359	0.389	0.388	0.409	0.389	0.411	0.383	0.407	0.387	0.407	0.559	0.515
ETTh1	96	0.307 \pm 0.001	0.345 \pm 0.002	<u>0.311</u>	<u>0.353</u>	0.319	0.358	0.318	0.355	0.319	0.360	0.318	0.356	0.334	0.368	0.329	0.367	0.345	0.372
	192	0.356 \pm 0.002	0.375 \pm 0.001	<u>0.356</u>	<u>0.378</u>	0.359	0.381	0.360	0.379	0.360	0.381	0.362	0.381	0.377	0.391	0.367	0.385	0.380	0.389
	336	0.391 \pm 0.003	0.399 \pm 0.002	<u>0.390</u>	<u>0.401</u>	0.391	0.404	0.393	0.402	0.389	0.403	0.393	0.404	0.426	0.420	0.399	0.410	0.413	0.413
	720	0.452 \pm 0.002	<u>0.437</u> \pm 0.003	0.452	0.440	0.470	0.436	0.449	0.440	0.447	0.441	0.460	0.442	0.491	0.459	0.454	0.439	0.474	0.453
	Avg	0.377 \pm 0.002	0.389 \pm 0.002	0.377	<u>0.393</u>	0.385	0.395	0.380	0.394	0.379	0.396	0.383	0.396	0.407	0.410	0.387	0.400	0.403	0.407
ETTh2	96	<u>0.168</u> \pm 0.001	<u>0.247</u> \pm 0.002	0.173	0.256	0.181	0.267	0.171	0.254	0.163	0.246	0.178	0.261	0.180	0.264	0.175	0.259	0.193	0.292
	192	<u>0.233</u> \pm 0.002	<u>0.291</u> \pm 0.001	0.238	0.298	0.243	0.306	0.235	0.302	0.229	0.290	0.243	0.303	0.250	0.309	0.241	0.302	0.284	0.362
	336	<u>0.289</u> \pm 0.003	<u>0.326</u> \pm 0.002	0.301	0.340	0.306	0.346	0.307	0.338	0.284	0.327	0.305	0.344	0.311	0.348	0.305	0.343	0.369	0.427
	720	0.384 \pm 0.002	0.385 \pm 0.003	0.397	0.396	0.407	0.399	0.403	0.395	0.389	0.391	0.393	0.397	0.412	0.407	0.402	0.400	0.554	0.522
	Avg	<u>0.269</u> \pm 0.002	0.312 \pm 0.002	0.277	0.323	0.284	0.329	0.279	0.322	0.266	0.314	0.280	0.326	0.288	0.332	0.281	0.326	0.350	0.401
Electricity	96	0.132 \pm 0.001	0.225 \pm 0.001	<u>0.134</u>	<u>0.229</u>	0.161	0.252	0.141	0.238	0.136	0.229	0.149	0.245	0.148	0.240	0.181	0.270	0.197	0.282
	192	0.150 \pm 0.002	0.242 \pm 0.001	0.154	0.247	0.172	0.261	0.157	0.251	<u>0.152</u>	<u>0.244</u>	0.165	0.260	0.162	0.253	0.188	0.274	0.196	0.285
	336	0.170 \pm 0.001	0.264 \pm 0.002	0.169	0.264	0.190	0.279	0.174	0.268	<u>0.170</u>	0.264	0.176	0.271	0.178	0.269	0.204	0.293	0.209	0.301
	720	0.184 \pm 0.002	0.278 \pm 0.001	<u>0.201</u>	<u>0.294</u>	0.231	0.313	0.209	0.303	0.212	0.299	0.204	0.296	0.225	0.317	0.246	0.324	0.245	0.333
	Avg	0.159 \pm 0.002	0.252 \pm 0.001	<u>0.164</u>	<u>0.259</u>	0.189	0.276	0.170	0.265	0.168	<u>0.259</u>	0.174	0.268	0.178	0.270	0.205	0.290	0.212	0.300
Solar-Energy	96	<u>0.187</u> \pm 0.002	0.215 \pm 0.001	0.173	0.233	0.216	0.258	0.197	0.236	0.190	0.247	0.186	<u>0.232</u>	0.203	0.237	0.234	0.286	0.290	0.378
	192	0.221 \pm 0.001	0.249 \pm 0.002	0.199	0.257	0.247	0.280	0.222	0.268	<u>0.210</u>	<u>0.266</u>	0.231	0.264	0.233	0.261	0.267	0.310	0.320	0.398
	336	0.234 \pm 0.002	<u>0.262</u> \pm 0.001	0.211	<u>0.263</u>	0.268	0.294	0.245	0.271	<u>0.217</u>	0.266	0.234	0.263	0.248	0.273	0.290	0.315	0.353	0.415
	720	0.244 \pm 0.001	<u>0.271</u> \pm 0.002	0.209	0.270	0.268	0.290	0.247	0.287	<u>0.223</u>	<u>0.266</u>	0.238	0.265	0.249	0.275	0.289	0.317	0.356	0.413
	Avg	0.222 \pm 0.002	0.249 \pm 0.002	0.198	<u>0.256</u>	0.250	0.281	0.228	0.266	<u>0.210</u>	0.261	0.222	0.256	0.233	0.262	0.270	0.307	0.330	0.401
Traffic	96	<u>0.411</u> \pm 0.002	<u>0.267</u> \pm 0.001	0.413	0.261	0.471	0.295	0.420	0.288	0.458	0.296	0.450	0.295	0.395	0.268	0.462	0.290	0.650	0.396
	192	<u>0.429</u> \pm 0.001	<u>0.276</u> \pm 0.002	0.432	0.271	0.480	0.300	0.434	0.298	0.457	0.294	0.489	0.311	0.417	<u>0.276</u>	0.466	0.290	0.598	0.370
	336	0.459 \pm 0.003	0.286 \pm 0.001	<u>0.450</u>	0.277	0.496	0.306	0.468	0.301	0.470	0.299	0.484	0.321	0.433	0.283	0.482	0.300	0.605	0.373
	720	<u>0.480</u> \pm 0.002	0.304 \pm 0.002	<u>0.486</u>	0.295	0.531	0.328	0.487	0.309	0.502	0.314	0.517	0.333	0.467	<u>0.302</u>	0.514	0.320	0.645	0.394
	Avg	<u>0.445</u> \pm 0.002	0.283 \pm 0.002	<u>0.445</u>	0.276	0.494	0.307	0.452	0.299	0.472	0.301	0.485	0.315	0.428	<u>0.282</u>	0.481	0.300	0.625	0.383
Weather	96	0.148 \pm 0.001	0.189 \pm 0.001	0.157	<u>0.200</u>	0.167	0.214	<u>0.156</u>	<u>0.204</u>	0.158	0.203	0.165	0.210	0.174	0.214	0.177	0.210	0.196	0.255
	192	0.200 \pm 0.002	0.241 \pm 0.001	0.206	<u>0.245</u>	0.215	0.255	<u>0.203</u>	<u>0.245</u>	0.207	0.247	0.212	0.253	0.221	0.254	0.225	0.250	0.237	0.296
	336	<u>0.256</u> \pm 0.001	0.284 \pm 0.002	0.262	0.287	0.270	0.294	0.250	0.284	0.262	0.289	0.267	0.293	0.278	0.296	0.278	0.290	0.283	0.335
	720	0.336 \pm 0.002	<u>0.339</u> \pm 0.001	0.344	0.342	0.346	0.344	<u>0.338</u>	0.337	0.344	0.344	0.344	0.342	0.358	0.349	0.354	0.340	0.345	0.381
	Avg	0.235 \pm 0.002	0.263 \pm 0.001	0.242	0.269	0.250	0.277	<u>0.237</u>	<u>0.268</u>	0.243	0.271	0.247	0.275	0.258	0.278	0.259	0.273	0.265	0.317

TABLE III

WORKLOAD FORECASTING RESULTS FOR ALL PREDICTION HORIZONS WITH FIXED LOOK-BACK $L = 96$. LOWER IS BETTER. BEST RESULTS ARE IN **BOLD**, SECOND BEST ARE UNDERLINED.

Dataset / H	AOSNET (Ours)			TQNet			CycleNet			iTransformer			
	MSE	MAE	NMAE	MSE	MAE	NMAE	MSE	MAE	NMAE	MSE	MAE	NMAE	
IaaS	96	0.754	0.596	0.748	<u>0.754</u>	<u>0.602</u>	<u>0.756</u>	0.756	0.604	0.759	0.905	0.684	0.859
	192	0.723	0.583	0.716	<u>0.740</u>	<u>0.588</u>	<u>0.722</u>	0.754	0.591	0.725	0.799	0.621	0.763
	336	0.726	0.577	0.701	0.746	0.592	0.719	<u>0.743</u>	<u>0.587</u>	<u>0.714</u>	0.810	0.627	0.762
	720	0.805	0.608	0.714	<u>0.848</u>	<u>0.630</u>	<u>0.741</u>	0.906	0.660	0.775	1.025	0.718	0.843
	Avg	0.752	0.591	0.720	<u>0.772</u>	<u>0.603</u>	<u>0.735</u>	0.790	0.610	0.743	0.885	0.662	0.807
PaaS	96	0.076	<u>0.144</u>	<u>0.186</u>	0.062	0.138	0.180	<u>0.074</u>	0.142	0.185	0.196	0.272	0.354
	192	0.139	0.170	0.181	<u>0.149</u>	<u>0.179</u>	<u>0.192</u>	0.145	0.178	0.191	0.346	0.341	0.365
	336	0.136	0.180	0.195	0.148	0.194							

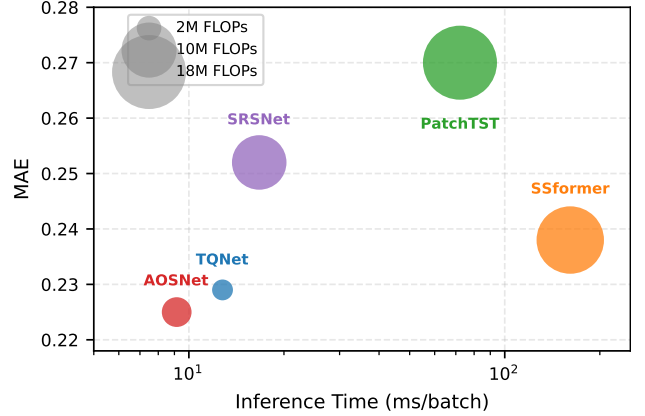
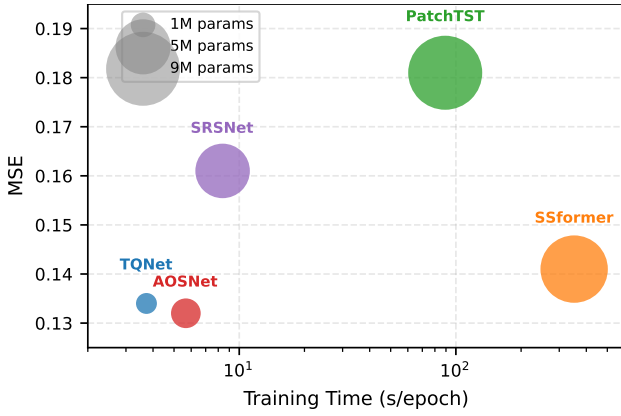


Fig. 4. Efficiency comparison on Electricity (look-back 96, horizon 96, batch size 32). Left: MSE vs. training time per epoch (bubble \propto parameters). Right: MAE vs. inference time per batch (bubble \propto FLOPs). AOSNET achieves the best accuracy with the fastest inference speed (9.15 ms/batch) and moderate model size (1.45M params).

compare AOSNET with CycleNet and TQNet under period settings $P \in \{12, 24, 36, 48\}$. The detailed generation procedure is described below.

For channel c and time index t , we define a base period $P_0 = 24$ and construct a time-varying amplitude $A_c(t)$, phase perturbation $\Delta\phi_c(t)$, and local period $P_c(t)$. The instantaneous angular frequency is

$$\omega_c(t) = \frac{2\pi}{P_c(t)}, \quad (25)$$

and the phase is accumulated as

$$\phi_c(t) = \phi_{c,0} + \sum_{\tau=1}^t \omega_c(\tau) + \Delta\phi_c(t), \quad (26)$$

where $\phi_{c,0}$ is a channel-specific random phase. The observed value is

$$x_c(t) = s_c [A_c(t) \sin \phi_c(t) + \rho_c A_c(t) \sin(2\phi_c(t) + \psi_c)] + r_c(t) + \epsilon_c(t), \quad (27)$$

where s_c is a channel scale, ρ_c controls a second harmonic, $r_c(t)$ is a weak trend and shared low-frequency component, and $\epsilon_c(t)$ is Gaussian noise.

The synthetic variants differ only in which oscillatory-state component is allowed to vary:

- **Stationary cycle:** $A_c(t) = 1$, $\Delta\phi_c(t) = 0$, and $P_c(t) = P_0$.
- **Amplitude modulation:** $A_c(t)$ varies smoothly while phase and period remain stable.
- **Phase drift:** $\Delta\phi_c(t)$ varies smoothly and includes a small random-walk component.
- **Local-frequency variation:** $P_c(t)$ varies smoothly around P_0 .
- **Combined non-stationary oscillation:** amplitude, phase, and local period all vary simultaneously.

The experiments in Table V use sequences of length 12000 with 16 channels. We train AOSNET and TQNet using the same look-back length $L = 96$ and horizon $H = 96$.

TQNet is evaluated with period choices $\{12, 24, 36, 48\}$, while AOSNET does not use a manually specified period.

2) *Results:* Table V reveals a clear pattern. On the stationary baseline (Syn-S), AOSNET already achieves the best MSE, confirming that oscillatory-state alignment does not hurt when templates happen to be sufficient. As non-stationarity increases—from pure amplitude modulation (Syn-A), to phase drift (Syn-P), to the combined setting (Syn-C)—AOSNET’s advantage over both CycleNet and TQNet grows consistently. Notably, CycleNet’s performance is largely insensitive to the period setting, indicating that its failure stems from the template assumption itself rather than period misspecification alone. TQNet’s attention-based template is more expressive, yet still degrades under phase drift (MSE changes from 0.019 at $P=24$ to 0.022 at $P=36$), whereas AOSNET requires no period specification.

3) *Stratified Analysis:* To further quantify this trend, we partition the test set into five quantile bins by per-sample non-stationarity score. Fig. 6 shows that CycleNet’s error remains $\sim 2\times$ that of AOSNET regardless of severity on Syn-A, while TQNet’s ratio increases monotonically from Q1 to Q5. This provides direct evidence that adaptive oscillatory-state alignment becomes increasingly advantageous as the local oscillatory state deviates further from a fixed template.

D. Oscillatory-State Alignment Analysis

We now examine the internal mechanism of AOSNET to verify that the model genuinely operates through oscillatory-state alignment rather than simply adding signal-processing features.

1) *The Prior is Not a Fixed Template:* Fig. 7 visualizes representative prior traces from the trained Electricity model. The curves exhibit oscillatory behavior—expected because the prior is optimized to provide meaningful amplitude, phase, and frequency references—but are not rigidly periodic: their amplitudes are uneven and local shapes vary. Fig. 8 further shows multiple spectral peaks, confirming that the prior stores a mixture of oscillatory scales rather than a single repeated cycle. This directly validates our design choice: the global

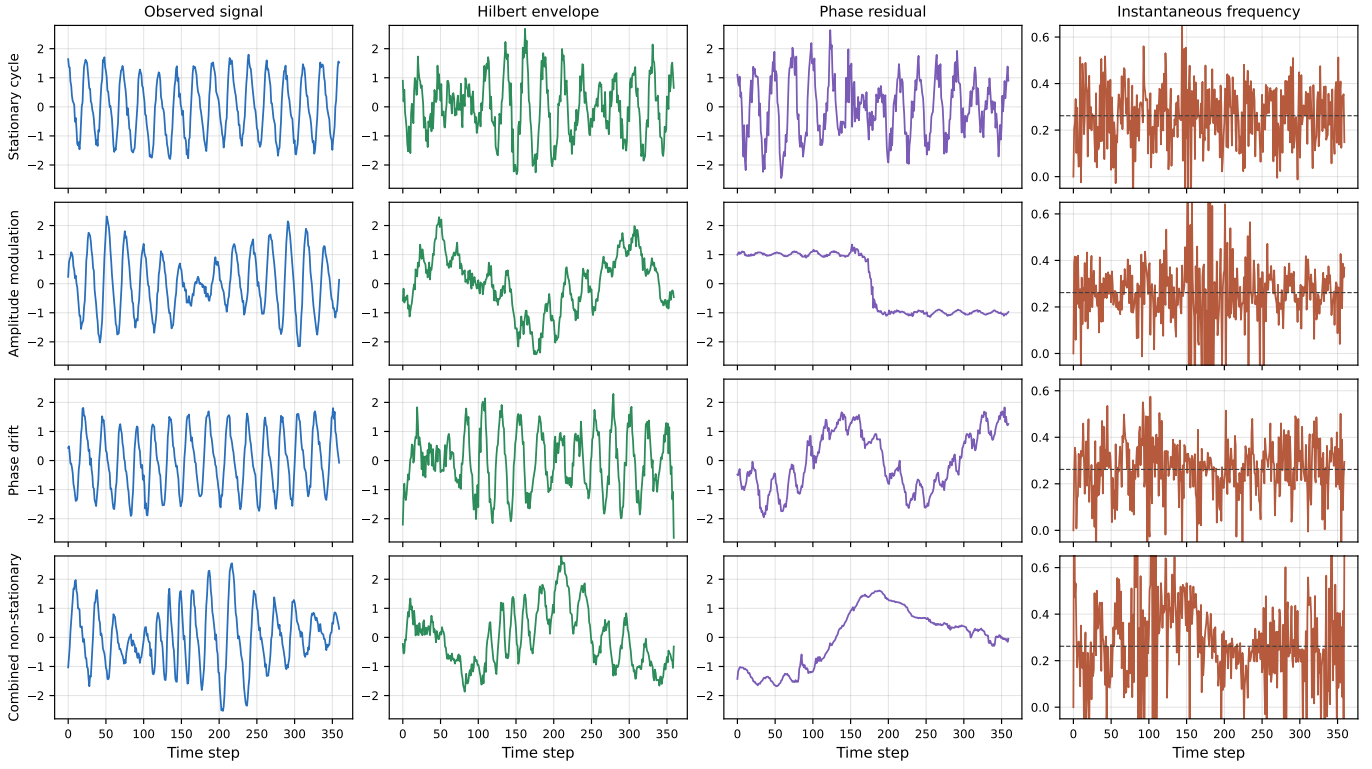


Fig. 5. Controlled synthetic variants and their Hilbert-domain characterization. Each row shows a representative signal, its envelope, phase residual relative to the base period, and instantaneous frequency. These descriptors directly correspond to the three failure modes: amplitude modulation changes the envelope, phase drift shifts the phase residual, and local-frequency variation alters the instantaneous frequency.

TABLE V
CONTROLLED SYNTHETIC RESULTS (LOOK-BACK 96, HORIZONS 96 AND 192). AOSNET REQUIRES NO PERIOD SPECIFICATION AND CONSISTENTLY OUTPERFORMS FIXED-TEMPLATE BASELINES, WITH GROWING ADVANTAGE AS NON-STATIONARITY INCREASES FROM SYN-S TO SYN-C.

Variant	H	AOSNET		CycleNet $P=12$		CycleNet $P=24$		CycleNet $P=36$		CycleNet $P=48$		TQNet $P=12$		TQNet $P=24$		TQNet $P=36$		TQNet $P=48$	
		MSE	MAE	MSE	MAE	MSE	MAE	MSE	MAE	MSE	MAE	MSE	MAE	MSE	MAE	MSE	MAE	MSE	MAE
Syn-S	96	0.013	0.089 _{±0.001}	0.021 _{±0.001}	0.115	0.021	0.115	0.022	0.116	0.021	0.115	0.014	0.095	0.015	0.098	0.017	0.102	0.015	0.098
	192	0.012	0.089 _{±0.002}	0.026 _{±0.001}	0.127	0.025	0.126	0.025	0.125	0.026	0.127	0.014	0.094	0.014	0.094	0.014	0.094	0.014	0.093
Syn-A	96	0.023	0.115 _{±0.001}	0.055 _{±0.001}	0.178	0.055	0.177	0.057	0.180	0.056	0.179	0.028	0.129	0.028	0.127	0.029	0.129	0.028	0.128
	192	0.024	0.116 _{±0.002}	0.061 _{±0.001}	0.191	0.056	0.184	0.060	0.189	0.060	0.190	0.025	0.122	0.026	0.125	0.025	0.122	0.028	0.130
Syn-P	96	0.017	0.104 _{±0.001}	0.032 _{±0.001}	0.142	0.032	0.142	0.033	0.145	0.032	0.142	0.021	0.114	0.019	0.109	0.022	0.116	0.019	0.110
	192	0.016	0.100 _{±0.002}	0.036 _{±0.001}	0.154	0.038	0.156	0.036	0.154	0.038	0.156	0.018	0.106	0.020	0.111	0.018	0.106	0.019	0.111
Syn-C	96	0.661	0.617 _{±0.001}	0.737 _{±0.001}	0.663	0.736	0.663	0.735	0.662	0.738	0.664	0.671	0.621	0.673	0.621	0.668	0.619	0.666	0.618
	192	0.746	0.669 _{±0.002}	0.817 _{±0.001}	0.709	0.821	0.711	0.818	0.710	0.823	0.711	0.774	0.682	0.767	0.678	0.771	0.681	0.777	0.682

oscillatory prior serves as a flexible reference that is adaptively interpreted through local state descriptors, not as a fixed periodic template to be retrieved by period indexing.

2) *The Gate Operates in Oscillatory-State Space*: Fig. 9 shows that the adaptive gate mainly responds to observed instantaneous frequency, phase, and amplitude descriptors, while prior descriptors provide the reference state. The gate thus performs state comparison in the Hilbert domain rather than simply copying the prior. The learned fusion coefficient is $\lambda=0.100$, meaning $\sim 90\%$ of prediction mass comes from the base projection of the aligned sequence—indicating that oscillatory-state alignment makes the temporal signal itself more predictable, rather than relying on the prior as a direct forecast.

3) *Oscillatory States Structure Cross-Variate Attention*: Fig. 10 shows that the cross-variate MHA preferentially attends to channels with stronger learned oscillatory priors. Combined with the ASR analysis (Table VI), this demonstrates that per-channel oscillatory-state alignment produces structurally refined representations that enable the downstream attention to discover meaningful cross-variate dependencies.

4) *Cross-Variate Dependency Analysis*: To quantify how oscillatory-state alignment structures cross-variate representations, we compute the Attention Structure Ratio (ASR):

$$\text{ASR} = \frac{\bar{A}_{\text{intra}}}{\bar{A}_{\text{inter}}}, \quad (28)$$

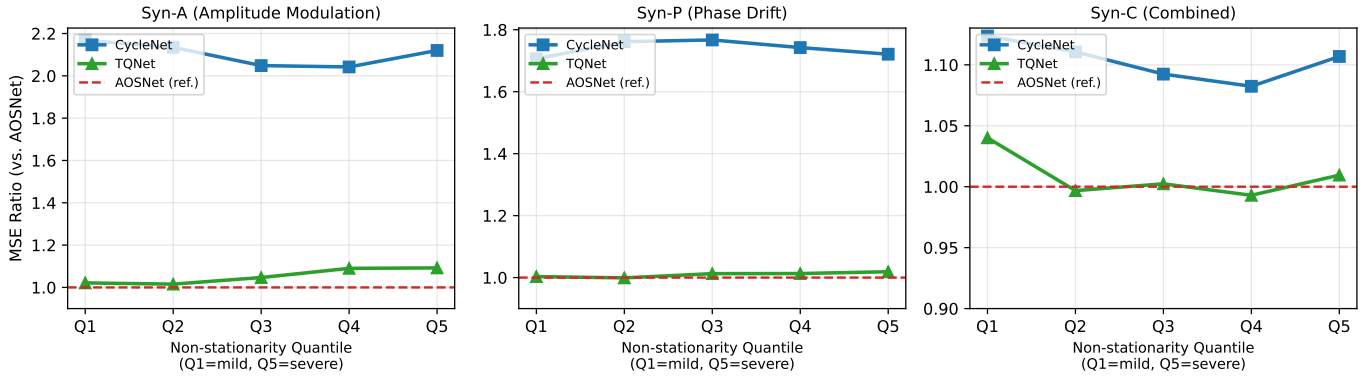


Fig. 6. Stratified evaluation by non-stationarity severity. Test samples are binned into five quantiles (Q1=mildest, Q5=most severe). The y -axis shows MSE ratio relative to AOSNET (dashed line at 1.0). TQNet’s disadvantage grows monotonically with severity on Syn-A (from $1.02\times$ to $1.09\times$), confirming that the advantage of oscillatory-state alignment is amplified under stronger state changes.

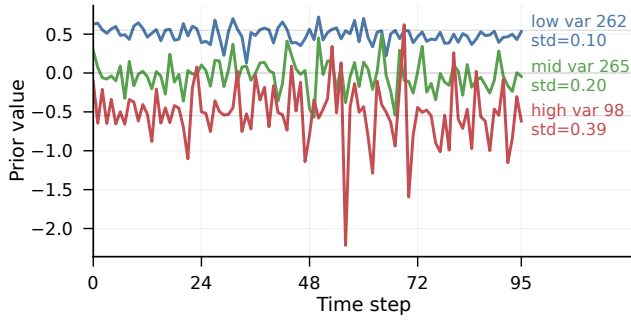


Fig. 7. Learned global oscillatory prior on Electricity. Variables are selected by prior standard deviation (low, median, high oscillation strength). The prior is oscillatory but not rigidly periodic: amplitudes are uneven and local shapes are nonuniform, confirming it functions as a flexible oscillatory reference rather than a fixed repeated template.

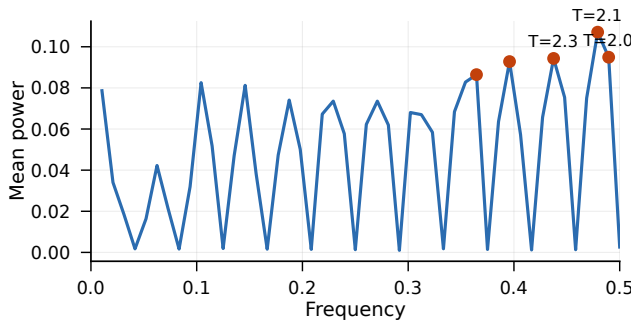


Fig. 8. Average spectrum of the learned prior. Multiple spectral peaks indicate that the prior captures a mixture of oscillatory scales rather than committing to a single predefined period.

where \bar{A}_{intra} and \bar{A}_{inter} denote average attention weights within and between K-Means clusters of channel embeddings.

As shown in Table VI, the full model achieves $\text{ASR} > 1.2$ on both datasets, while removing AOS causes ASR to drop below 1.0 on Electricity. This confirms that oscillatory-state alignment is critical for structuring the input so that the MHA can discover cross-variate dependencies.

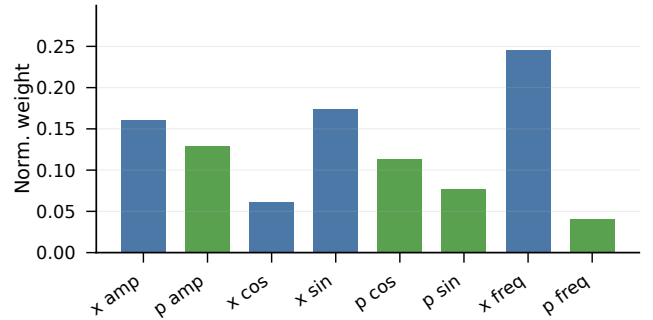


Fig. 9. Effective descriptor weights in the adaptive gate. The gate primarily responds to observed instantaneous frequency, phase, and amplitude, using the prior descriptors as the reference state for comparison.

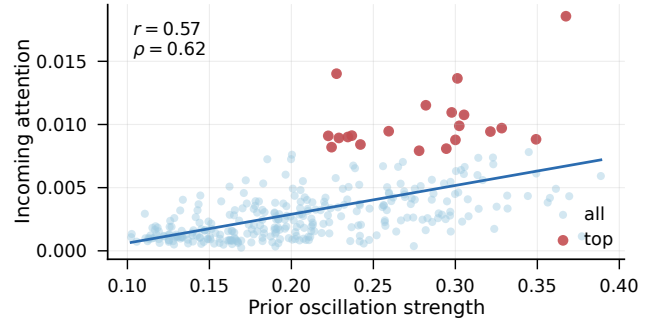


Fig. 10. Relation between prior oscillation strength and incoming channel attention. Variables with stronger oscillatory priors receive more cross-variate attention, suggesting that oscillatory-state alignment creates informative channel representations.

E. Case Study: Same Phase, Different States

Fig. 11 provides a case study that crystallizes the conceptual difference between fixed-template periodicity and oscillatory-state alignment. Multiple observed windows in the Syn-C dataset start from the same cycle phase, yet their local oscillatory states—as revealed by envelope, phase residual, and instantaneous frequency—differ substantially. A period-indexed method (CycleNet, TQNet) must assign identical templates to

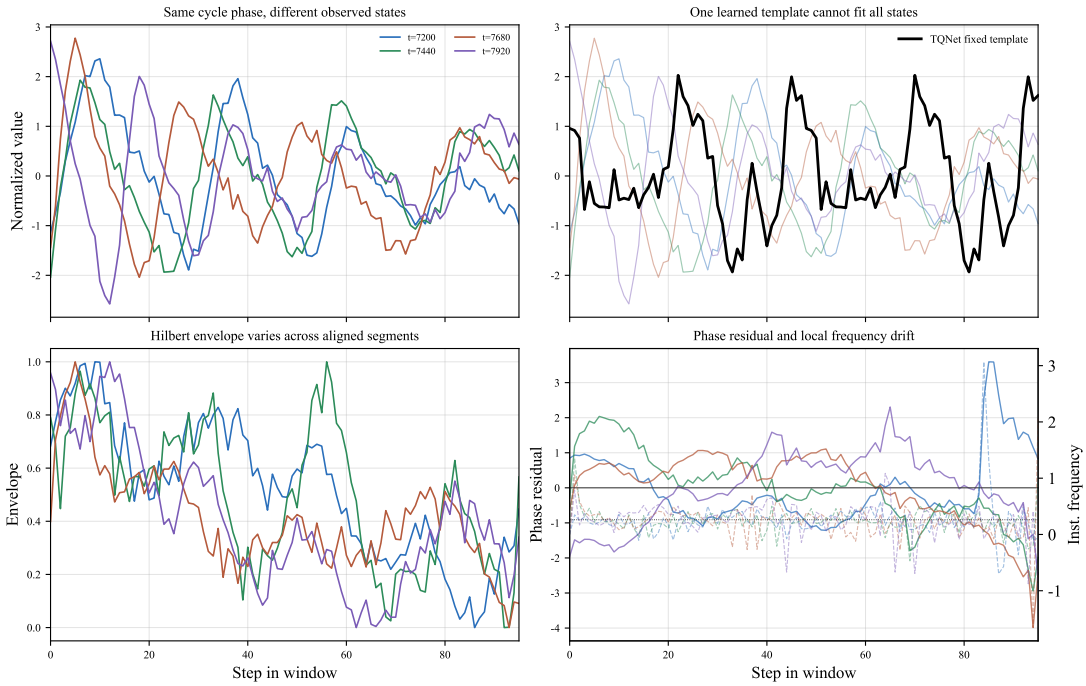


Fig. 11. Failure of fixed-template retrieval on the combined non-stationary dataset. Top-left: windows starting from the same cycle phase exhibit different local shapes. Top-right: TQNet assigns the same template to all phase-aligned windows. Bottom: Hilbert descriptors reveal that envelope, phase residual, and instantaneous frequency all differ across these windows. This demonstrates the fundamental limitation of period-indexed template retrieval: same cycle phase does not imply the same oscillatory state.

TABLE VI
ATTENTION STRUCTURE RATIO (ASR) WITH AND WITHOUT AOS. ASR > 1 INDICATES STRUCTURED CROSS-VARIATE ATTENTION; ASR ≤ 1 INDICATES UNIFORM ATTENTION.

Variant	Electricity (321 ch.)		Weather (21 ch.)	
	ASR	$\bar{A}_{intra}/\bar{A}_{inter}$	ASR	$\bar{A}_{intra}/\bar{A}_{inter}$
AOSNET (full)	1.208	0.00342/0.00283	1.213	0.0532/0.0439
w/o AOS	0.716	0.00257/0.00359	0.971	0.0472/0.0486

all phase-aligned windows, because the template is retrieved solely by the period index. In contrast, AOSNET reads the local oscillatory state of each window and adapts its alignment accordingly. This illustrates the core insight: *same cycle phase does not imply same oscillatory state*, which is precisely why fixed periodic indexing fails under non-stationary dynamics.

Fig. 12 further visualizes representative forecasts. On Syn-A and Syn-P, the fixed-template baselines produce periodic predictions that diverge when the local state deviates from the training-set average, whereas AOSNET adapts its forecast to the instantaneous oscillatory state.

F. Ablation and Sensitivity

1) *Ablation*: Table VII validates the contribution of each component. The AOS module is consistently beneficial (+3.3% to +14.2%), with the largest gains on datasets with complex oscillatory dynamics (Weather +14.2%, Electricity +9.8%). The global oscillatory prior shows a similar pattern

TABLE VII
ABLATION STUDY (LOOK-BACK 96, HORIZON 96). $\Delta\%$ DENOTES RELATIVE MSE DEGRADATION FROM THE FULL MODEL.

Variant	ETTh1			ETTm1			Electricity			Weather		
	MSE	MAE	$\Delta\%$	MSE	MAE	$\Delta\%$	MSE	MAE	$\Delta\%$	MSE	MAE	$\Delta\%$
AOSNET (full)	0.368	0.392	-	0.307	0.345	-	0.132	0.225	-	0.148	0.189	-
w/o AOS	0.380	0.398	+3.3	0.319	0.353	+3.9	0.145	0.234	+9.8	0.169	0.206	+14.2
w/o Prior	0.375	0.393	+1.9	0.321	0.355	+4.6	0.145	0.234	+9.8	0.171	0.208	+15.5
w/o MHA	0.365	0.390	-0.8	0.315	0.350	+2.6	0.150	0.238	+13.6	0.162	0.202	+9.5
w/o Fusion	0.380	0.389	+3.3	0.327	0.358	+6.5	0.180	0.265	+36.4	0.165	0.208	+11.5
w/o Amp	0.370	0.393	+0.5	0.316	0.348	+2.9	0.133	0.227	+1.5	0.153	0.195	+3.4
w/o Phase	0.371	0.393	+0.8	0.313	0.348	+2.0	0.135	0.228	+2.3	0.149	0.190	+0.5
w/o IF	0.369	0.390	+0.3	0.315	0.350	+2.6	0.134	0.228	+1.5	0.149	0.192	+0.5

(+15.5% on Weather), confirming that the learned reference provides meaningful oscillatory-state information. Dual-path fusion is critical on high-dimensional data (Electricity +36.4%), while cross-variate MHA is indispensable on multi-channel datasets (+13.6% on Electricity) but neutral on the 7-channel ETTh1. Among the three analytic-signal descriptors, all contribute complementarily, with log-amplitude most impactful on Weather (+3.4%).

2) *Sensitivity*: Fig. 13 shows that AOSNET is robust to both model dimension and kernel size, with performance remaining nearly flat across the full tested range. Even reducing d_{model} to 128 ($4\times$ fewer parameters) incurs at most $\sim 1\%$ MSE increase, making the model suitable for resource-constrained deployment. Fig. 14 further shows that AOSNET achieves the best MSE at every tested look-back length (96–720) on Electricity. All methods improve with longer windows as

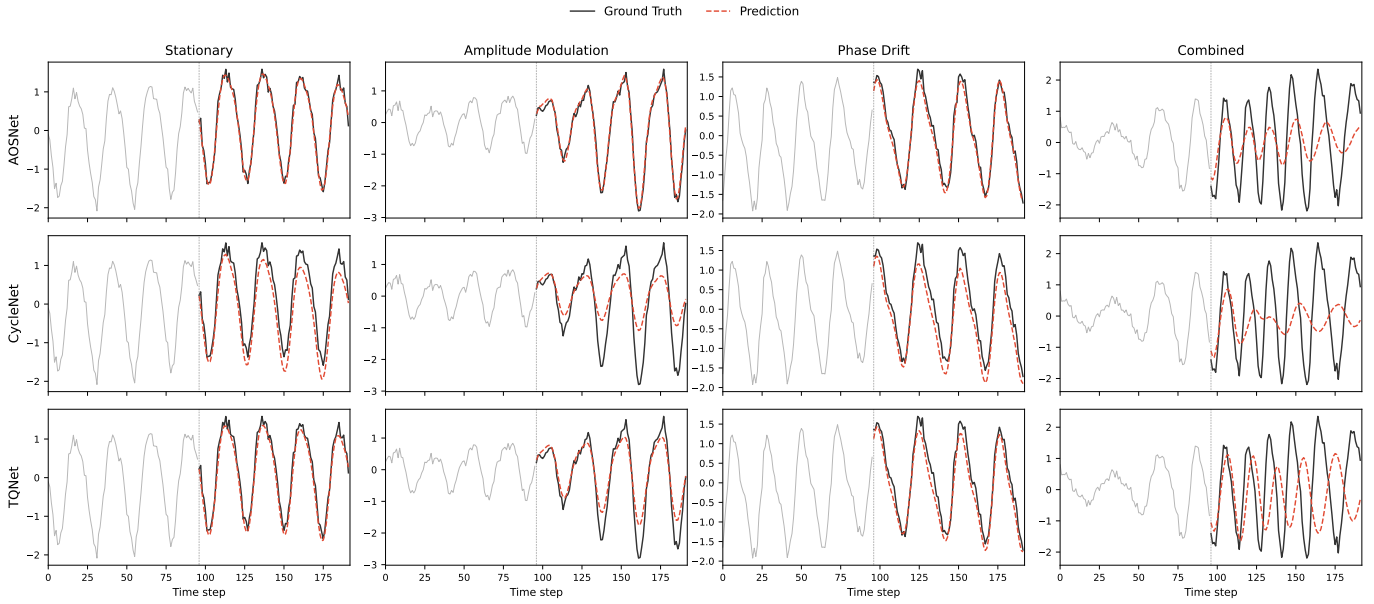


Fig. 12. Prediction visualization on four synthetic datasets (look-back 96, horizon 96). AOSNET tracks envelope changes (Syn-A), phase shifts (Syn-P), and their combination (Syn-C), while CycleNet and TQNet produce rigidly periodic predictions that fail to adapt to evolving oscillatory states.

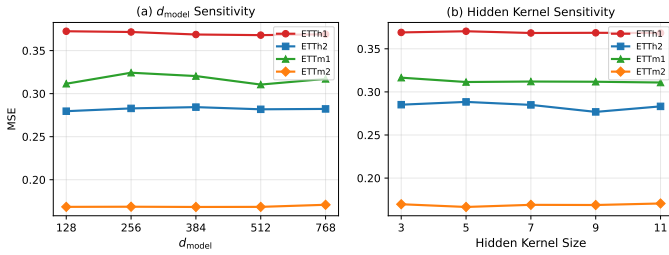


Fig. 13. Parameter sensitivity on four ETT datasets (horizon 96). (a) Varying $d_{\text{model}} \in \{128, 256, 384, 512, 768\}$ with kernel fixed at 5. (b) Varying kernel size $\in \{3, 5, 7, 9, 11\}$ with $d_{\text{model}}=512$. Performance remains within $\pm 5\%$ across all settings.

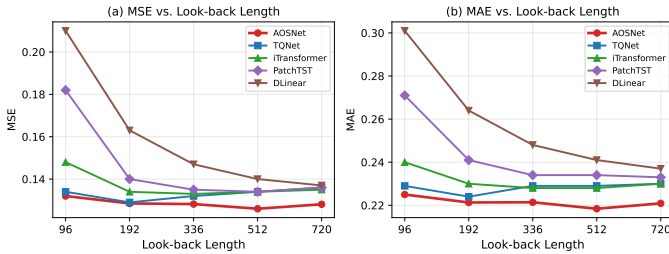


Fig. 14. Look-back length sensitivity on Electricity (horizon 96). All methods benefit from longer look-back windows, as expected. AOSNET achieves the lowest MSE at every tested length and already performs strongly at $L=96$, whereas PatchTST and DLinear require substantially longer windows to become competitive.

expected; AOSNET already performs strongly at the shortest setting ($L=96$), while PatchTST and DLinear require $L \geq 336$ to approach comparable accuracy.

VI. CONCLUSION AND LIMITATIONS

We presented AOSNET, a Hilbert-guided forecasting model that reformulates explicit periodic modeling from fixed template matching to adaptive oscillatory-state alignment. Instead of requiring a predefined period or a globally stable repeated pattern, AOSNET extracts envelope, phase, and instantaneous-frequency descriptors from both the observed sequence and a learnable global temporal prior. A lightweight adaptive gate then uses these local descriptors to decide where the observation should be preserved and where it should be softly corrected toward the learned reference. Controlled experiments show that this design is especially useful when amplitude, phase, or local frequency changes over time, and model analysis suggests that the learned prior acts as an oscillatory reference rather than a hard periodic template.

Limitations and Future Work.: The current study focuses on point forecasting with a compact backbone, so the benefit of adaptive oscillatory states has not yet been fully explored in larger Transformer-style architectures or probabilistic forecasting settings. The Hilbert descriptors are computed along fixed look-back windows, which may be less suitable when useful oscillatory structure appears at multiple resolutions or across irregularly sampled observations. In addition, the global temporal prior is shared across samples; while this provides a simple dataset-level reference, future work could make the prior conditional on covariates, regimes, or cluster-level temporal states. Finally, the current experiments emphasize standard benchmarks and controlled non-stationary oscillations. A broader evaluation on domain-specific datasets with abrupt regime changes, missing values, and exogenous events would further clarify when adaptive oscillatory-state alignment is most beneficial.

REFERENCES

- [1] Q. Wen, T. Zhou, C. Zhang, W. Chen, Z. Ma, J. Yan, and L. Sun, "Transformers in Time Series: A Survey," *arXiv preprint arXiv:2202.07125*, 2022.
- [2] X. Qiu, J. Hu, L. Zhou, X. Wu, J. Du, B. Zhang, C. Guo, A. Zhou, C. S. Jensen, Z. Sheng, and B. Yang, "TFB: Towards Comprehensive and Fair Benchmarking of Time Series Forecasting Methods," in *International Conference on Very Large Data Bases (VLDB)*, Guangzhou, China, Aug. 26-30, 2024.
- [3] Z. Shao, F. Wang, Y. Xu, W. Wei, C. Yu, Z. Zhang, D. Yao, T. Sun, G. Jin, X. Cao, G. Cong, C. S. Jensen, and X. Cheng, "Exploring Progress in Multivariate Time Series Forecasting: Comprehensive Benchmarking and Heterogeneity Analysis," *IEEE Transactions on Knowledge and Data Engineering*, vol. 37, pp. 291–305, Jan. 2025.
- [4] Q. Guo, B. Zhao, M. Song, and G. Zhong, "A Survey of Deep Learning for Time Series Forecasting: Taxonomy, Analysis and Future Directions," *IEEE Transactions on Knowledge and Data Engineering*, pp. 1–20, 2026.
- [5] H. Zhou, S. Zhang, J. Peng, S. Zhang, J. Li, H. Xiong, and W. Zhang, "Informer: Beyond Efficient Transformer for Long Sequence Time-Series Forecasting," in *Proceedings of The AAAI Conference on Artificial Intelligence*, Virtual Event, Feb. 2-9, 2021.
- [6] A. Zeng, M. Chen, L. Zhang, and Q. Xu, "Are Transformers Effective for Time Series Forecasting?" in *Proceedings of The AAAI Conference on Artificial Intelligence*, Washington, DC, USA, Feb. 7-14, 2023.
- [7] X. Zhang, Z. Huang, Y. Wu, X. Lu, E. Qi, Y. Chen, Z. Xue, Q. Wang, P. Wang, and W. Wang, "Multi-Period Learning for Financial Time Series Forecasting," in *Proceedings of The 31st ACM SIGKDD Conference on Knowledge Discovery and Data Mining*, Toronto, ON, Canada, Aug. 3-7, Jul. 2025, pp. 2848–2859. [Online]. Available: <http://arxiv.org/abs/2511.08622>
- [8] L. Chen, X. Zhong, F. Zhang, Y. Cheng, Y. Xu, Y. Qi, and H. Li, "FuXi: A Cascade Machine Learning Forecasting System for 15-Day Global Weather Forecast," *npj Climate and Atmospheric Science*, vol. 6, no. 1, p. 190, Nov. 2023.
- [9] H. Wu, J. Xu, J. Wang, and M. Long, "Autoformer: Decomposition Transformers with Auto-Correlation for Long-Term Series Forecasting," in *Annual Conference on Neural Information Processing Systems (NeurIPS)*, Virtual, Dec. 6-14, 2021.
- [10] Y. Nie, N. H. Nguyen, P. Sinthong, and J. Kalagnanam, "A Time Series Is Worth 64 Words: Long-Term Forecasting with Transformers," in *International Conference on Learning Representations (ICLR)*, Kigali, Rwanda, May 1-5, 2023.
- [11] Y. Liu, T. Hu, H. Zhang, H. Wu, S. Wang, L. Ma, and M. Long, "iTransformer: Inverted Transformers Are Effective for Time Series Forecasting," in *International Conference on Learning Representations (ICLR)*, Vienna, Austria, May 7-11, 2024.
- [12] W. Ye, S. Deng, Q. Zou, and N. Gui, "Frequency Adaptive Normalization for Non-Stationary Time Series Forecasting," in *Annual Conference on Neural Information Processing Systems (NeurIPS)*, Vancouver, BC, Canada, Dec. 10 - 15, 2024.
- [13] P. Liu, B. Wu, Y. Hu, N. Li, T. Dai, J. Bao, and S.-T. Xia, "TimeBridge: Non-Stationarity Matters for Long-Term Time Series Forecasting," in *International Conference on Machine Learning (ICML)*, Vancouver, Canada, Jul. 13-19, 2025.
- [14] Z. Song, X. Zhang, L. Zhuang, T. Guo, X. Zhao, Y. Xu, and S. Jin, "Diffusion-based spatio-temporal channel prediction via non-stationarity decoupling," *IEEE Transactions on Cognitive Communications and Networking*, vol. 12, pp. 7647–7661, 2026.
- [15] S. Lin, W. Lin, X. Hu, W. Wu, R. Mo, and H. Zhong, "CycleNet: Enhancing Time Series Forecasting through Modeling Periodic Patterns," in *Annual Conference on Neural Information Processing Systems (NeurIPS)*, Vancouver, Canada, Dec. 9-15, 2024.
- [16] S. Lin, H. Chen, H. Wu, C. Qiu, and W. Lin, "Temporal Query Network for Efficient Multivariate Time Series Forecasting," in *International Conference on Machine Learning (ICML)*, ser. Proceedings of Machine Learning Research, vol. 267. BC, Canada, Jul. 13-19: PMLR / OpenReview.net, 2025. [Online]. Available: <https://proceedings.mlr.press/v267/lin25e.html>
- [17] T. Zhou, Z. Ma, Q. Wen, L. Sun, T. Yao, W. Yin, R. Jin *et al.*, "FILM: Frequency Improved Legendre Memory Model for Long-Term Time Series Forecasting," in *Annual Conference on Neural Information Processing Systems (NeurIPS)*, LA, USA, Nov. 28-Dec. 9, 2022.
- [18] H. Wang, L. Pan, Y. Shen, Z. Chen, D. Yang, Y. Yang, S. Zhang, X. Liu, H. Li, and D. Tao, "FreDF: Learning to Forecast in The Frequency Domain," in *International Conference on Learning Representations (ICLR)*, Singapore, Apr. 24-28, 2025. [Online]. Available: <https://openreview.net/forum?id=4A9ldSa1ul>
- [19] J. Fei, K. Yi, W. Fan, Q. Zhang, and Z. Niu, "Amplifier: Bringing Attention to Neglected Low-Energy Components in Time Series Forecasting," in *Proceedings of The AAAI Conference on Artificial Intelligence*, Philadelphia, PA, USA, Feb. 25 - Mar. 4, 2025. [Online]. Available: <https://doi.org/10.1609/aaai.v39i11.33267>
- [20] S. Wang, H. Wu, X. Shi, T. Hu, H. Luo, L. Ma, J. Y. Zhang, and J. Zhou, "TimeMixer: Decomposable Multiscale Mixing for Time Series Forecasting," in *International Conference on Learning Representations (ICLR)*, Vienna, Austria, May 7-11, 2024.
- [21] G. Yu, J. Zou, X. Hu, A. I. Aviles-Rivero, J. Qin, and S. Wang, "Revitalizing Multivariate Time Series Forecasting: Learnable Decomposition with Inter-Series Dependencies and Intra-Series Variations Modeling," in *International Conference on Machine Learning (ICML)*, Vienna, Austria, Jul. 21-27, 2024.
- [22] J. Deng, F. Ye, D. Yin, X. Song, I. Tsang, and H. Xiong, "Parsimony or Capability? Decomposition Delivers Both in Long-Term Time Series Forecasting," in *Annual Conference on Neural Information Processing Systems (NeurIPS)*, Vancouver, Canada, Dec. 9-15, 2024.
- [23] D. Gabor, "Theory of Communication," *Journal of the Institution of Electrical Engineers*, vol. 93, no. 26, pp. 429–457, 1946.
- [24] B. Boashash, "Estimating and Interpreting the Instantaneous Frequency of a Signal. I. Fundamentals," *Proceedings of the IEEE*, vol. 80, no. 4, pp. 520–568, 1992.
- [25] T. Zhou, Z. Ma, Q. Wen, X. Wang, L. Sun, and R. Jin, "FED-Former: Frequency Enhanced Decomposed Transformer for Long-Term Series Forecasting," in *International Conference on Machine Learning (ICML)*, Baltimore, MD, Jul. 17-23, 2022.
- [26] H. Wang, J. Peng, F. Huang, J. Wang, J. Chen, and Y. Xiao, "MICN: Multi-Scale Local and Global Context Modeling for Long-Term Series Forecasting," in *International Conference on Learning Representations (ICLR)*, Kigali, Rwanda, May 1-5, 2023.
- [27] S. Lin, W. Lin, W. Wu, H. Chen, and J. Yang, "SparseTSF: Modeling Long-Term Time Series Forecasting with *1k* Parameters," in *International Conference on Machine Learning (ICML)*, ser. Proceedings of Machine Learning Research, vol. 235. Vienna, Austria, Jul. 21-27: PMLR / OpenReview.net, 2024, pp. 30211–30226. [Online]. Available: <https://proceedings.mlr.press/v235/lin24n.html>
- [28] J. Ma, B. Wang, Q. Huang, G. Wang, P. Wang, Z. Zhou, and Y. Wang, "MoFo: Empowering Long-Term Time Series Forecasting with Periodic Pattern Modeling," in *Annual Conference on Neural Information Processing Systems (NeurIPS)*, San Diego, CA, USA, Dec. 2-7, 2026. [Online]. Available: <https://openreview.net/forum?id=sbvLts2HqR>
- [29] Z. Xu, A. Zeng, and Q. Xu, "FITS: Modeling Time Series with 10K Parameters," in *International Conference on Learning Representations (ICLR)*, Vienna, Austria, May 7-11, 2024.
- [30] A. Vaswani, N. Shazeer, N. Parmar, J. Uszkoreit, L. Jones, A. N. Gomez, L. Kaiser, and I. Polosukhin, "Attention Is All You Need," in *Annual Conference on Neural Information Processing Systems (NeurIPS)*, Long Beach, California, USA, Dec. 4-9, 2017.
- [31] Z. Song, N. Jiang, M. He, X. Zhao, and T. Guo, "Channel, Trend and Periodic-Wise Representation Learning for Multivariate Long-Term Time Series Forecasting," in *International Conference on Acoustics, Speech and Signal Processing (ICASSP)*. Barcelona, Spain, May 4-8: IEEE, 2026, pp. 4821–4825.
- [32] L. Han, H.-J. Ye, and D.-C. Zhan, "The Capacity and Robustness Trade-Off: Revisiting The Channel Independent Strategy for Multivariate Time Series Forecasting," *IEEE Transactions on Knowledge and Data Engineering*, 2024.
- [33] Y. Zhang and J. Yan, "Crossformer: Transformer Utilizing Cross-Dimension Dependency for Multivariate Time Series Forecasting," in *International Conference on Learning Representations (ICLR)*, Kigali, Rwanda, May 1-5: OpenReview.net, 2023. [Online]. Available: <https://openreview.net/forum?id=vSVLM2j9eie>
- [34] Q. Huang, L. Shen, R. Zhang, J. Cheng, S. Ding, Z. Zhou, and Y. Wang, "HDMixer: Hierarchical Dependency with Extendable Patch for Multivariate Time Series Forecasting," in *Proceedings of The AAAI Conference on Artificial Intelligence*, Vancouver, Canada, Feb. 20-27, 2024.

- [35] R. Ilbert, A. Odonnat, V. Feofanov, A. Virmaux, G. Paolo, T. Palpanas, and I. Redko, "SAMformer: Unlocking The Potential of Transformers in Time Series Forecasting with Sharpness-Aware Minimization and Channel-Wise Attention," in *International Conference on Machine Learning (ICML)*, vol. 235. Vienna, Austria, Jul. 21-27: PMLR, 2024. [Online]. Available: <https://proceedings.mlr.press/v235/ilbert24a.html>
- [36] E. O. Brigham and R. E. Morrow, "The Fast Fourier Transform," *IEEE Spectrum*, 1967.
- [37] D. Hendrycks and K. Gimpel, "Gaussian Error Linear Units (GELUs)," *arXiv preprint arXiv:1606.08415*, 2016.
- [38] N. Srivastava, G. Hinton, A. Krizhevsky, I. Sutskever, and R. Salakhutdinov, "Dropout: A Simple Way to Prevent Neural Networks from Overfitting," *Journal of Machine Learning Research*, vol. 15, no. 56, pp. 1929–1958, 2014.
- [39] A. Paszke, S. Gross, F. Massa, A. Lerer, J. Bradbury, G. Chanan, T. Killeen, Z. Lin, N. Gimelshein, L. Antiga *et al.*, "Pytorch: An Imperative Style, High-Performance Deep Learning Library," in *Annual Conference on Neural Information Processing Systems (NeurIPS)*, Vancouver, Canada, Dec. 8-14, 2019.
- [40] X. Wu, X. Qiu, H. Cheng, Z. Li, J. Hu, C. Guo, and B. Yang, "Enhancing Time Series Forecasting through Selective Representation Spaces: A Patch Perspective," in *Annual Conference on Neural Information Processing Systems (NeurIPS)*, Vancouver, Canada, Dec. 9-14, 2025.
- [41] Y. Liu, B. Liu, S. Huang, G. Luo, W. Hu, M. Wang, and R. Hong, "Sparse-scale transformer with bidirectional awareness for time series forecasting," in *Proceedings of The AAAI Conference on Artificial Intelligence*. Singapore, January 20-27: AAAI Press, 2026, pp. 23 899–23 907. [Online]. Available: <https://doi.org/10.1609/aaai.v40i28.39566>